Research Article | Vol. 31, No. 21 / 9 Oct 2023 / Optics Express 34688
Optics EXPRESS

Fabry-Perot Bragg grating nanoresonator with ultrahigh intrinsic Q based on low-loss silicon nitride

YANG ZHANG,[1] SYLVAIN VEILLEUX,[2] AND MARIO DAGENAIS[1,*]

[1]Department of Electrical and Computer Engineering, University of Maryland, College Park, MD 20742, USA
[2]Department of Astronomy, University of Maryland, College Park, MD 20742, USA
*dage@umd.edu

Abstract: Photonic integrated circuits based on ultralow loss silicon nitride waveguides have shown significant promise for realizing high-performance optical systems in a compact and scalable form factor. For the first time, we have developed a Fabry-Perot Bragg grating nanoresonator based on silicon nitride on silicon dioxide platform with an ultra-high intrinsic quality factor of 19.3 million. By combining the introduction of tapered grating between cavity and periodic Bragg grating, increasing the width of cavity to multi-mode region and optimized annealing strategy for Si_3N_4 film, the propagation loss is reduced to around 0.014 dB/cm. Fabry-Perot Bragg grating nanoresonator can be easily implemented in a simple straight waveguide occupying a minimal amount of space. Therefore, it is a key component to build a high performance photonic integrated circuit for many applications.

1. Introduction

In the past decade, photonic integrated circuits (PICs) have emerged as a promising technology for realizing high-performance optical systems in a compact and scalable form factor. Unlike traditional discrete optical components, which require extensive alignment and assembly, PICs enable the integration of multiple optical functions on a single chip, resulting in reduced size, weight, power consumption, and cost.

The key building blocks of a PIC typically include waveguides, couplers, filters, modulators, detectors, and amplifiers, which can be fabricated using various materials and technologies, such as silicon, silicon nitride, indium phosphide, gallium arsenide, and lithium niobate. The choice of material and technology depends on the specific requirements of the PIC, such as the operating wavelength, bandwidth, polarization, and temperature range, as well as the manufacturing process and cost. Among them, the silicon nitride (Si_3N_4) platform offers a unique combination of low loss, high nonlinearity, large mode area, and CMOS compatibility, making them well-suited for a wide range of applications in optical communications, sensing, computing, quantum optics, and astrophotonics. The key advantage of Si_3N_4 waveguides is their exceptionally low propagation loss, which can be less than 1 dB m^{-1} [1–3], depending on the waveguide dimensions and fabrication process. This is orders of magnitude lower than the losses of traditional waveguides based on silicon on insulator (SOI), and enables high-quality-factor resonators [1,4,5], long-distance delays, and low-threshold nonlinear effects [6–8]. Moreover, Si_3N_4 waveguides exhibit low polarization-dependent loss, high thermal stability, and compatibility with standard CMOS fabrication processes, making them highly attractive for integration with electronics and other optical components.

Despite these advancements, several challenges remain in the design, fabrication, and integration of Si_3N_4-based PICs, such as the optimization of the waveguide dimensions and materials to achieve the desired performance, the mitigation of fabrication imperfections and

#499930 https://doi.org/10.1364/OE.499930
Journal © 2023 Received 5 Jul 2023; revised 19 Aug 2023; accepted 19 Aug 2023; published 2 Oct 2023

Optics EXPRESS

variations, and the integration with other optical and electronic components. In our work, an ultrahigh quality factor Q_{int} of 19.3 million based on a Fabry-Perot Bragg grating (FPBG) nanoresonator is demonstrated for the first time. Using an efficient approach based on measuring the transmission of on-chip Fabry-Perot cavities with various lengths [9,10], we have extracted the loss of 0.014 dB/cm in our Si_3N_4 film. Compared to the waveguide-coupled ring resonators, FPBG resonators require less engineering in the coupling region and have no bending losses. This structure is particularly suitable for producing high Q resonances in the low-confinement Si_3N_4 waveguide platform, which can be designed to be compact in size. The parameters of FPBG resonators, such as the grating period and the refractive index modulation, can be precisely engineered to control the spectral response, which enables tailoring the resonator's behavior to specific wavelength ranges or applications, offering flexibility in meeting diverse requirements. FPBGs can also be adapted across multiple functions for various applications, including optical filters [11], wavelength multiplexers/demultiplexers [12], sensors [13], and modulators [14].

The paper is organized as follows. In the following section, we will first briefly discuss the theory and design for the high-Q FPBG. In Section 3, we will provide the details of the fabrication process of the device, and the measurement set-up. The performance of fabricated devices will be analyzed in Section 4. Finally, the outlook towards future development and conclusions will be given in Section 5.

2. Theory

A Fabry-Perot Bragg grating is an optical resonator that combines the properties of a Fabry-Perot cavity and a Bragg grating. It consists of a waveguide between two partially reflective mirrors consisting of a Bragg grating. The Bragg grating provides wavelength-selective feedback, allowing only certain wavelengths to be coupled back into the waveguide and reinforcing the resonant mode. The resonant wavelength of the FPBG is determined by the cavity length and the grating period. By changing the cavity length or the refractive index of the waveguide, the resonant wavelength can be tuned. The quality factor of the resonator, which represents the energy storage and dissipation within the cavity, is determined by the reflectivity of the mirrors, the loss in the waveguide, and the coupling efficiency of the grating.

To extract the accurate loss of the Si_3N_4 waveguide, two methods are used to fit the experimental data. One method uses a transfer matrix method to simulate the transmission of the cavity [9], and the other method uses a fit of the quality factor Q_{load} as a function of cavity lengths [15,16].

2.1. ABCD transfer matrix model

The waveguide Bragg grating that we will focus on in this work is an optical waveguide device with a periodic variation of the refractive index along the propagation direction, as shown in Fig. 1(a). The corrugated grating on the sides of the waveguide (fishbone structure) with period Λ is patterned by electron beam lithography (EBL). Constructive interference between different reflections occurs when the optical path difference is an integral number of wavelength λ_0/n_{eff} in the waveguide, that is the period of the grating satisfy the following Bragg condition,

$$\Lambda = \frac{m\lambda_0}{2n_{eff}}, \quad m = 1,\ 2,\ 3, \ldots \tag{1}$$

where λ_0 is the vacuum wavelength of light, and n_{eff} is the group index of the waveguide. It includes both the average index and the index variation with wavelength. This waveguide Bragg grating can also be considered as a diffraction grating which diffracts the forward-travelling wave into a backward-traveling wave.

In the periodic waveguide Bragg gratings, the alternating layers with two different refractive indices can be treated as a unit cell, see Fig. 1(b). Since the optical wave is guided within the

Optics EXPRESS

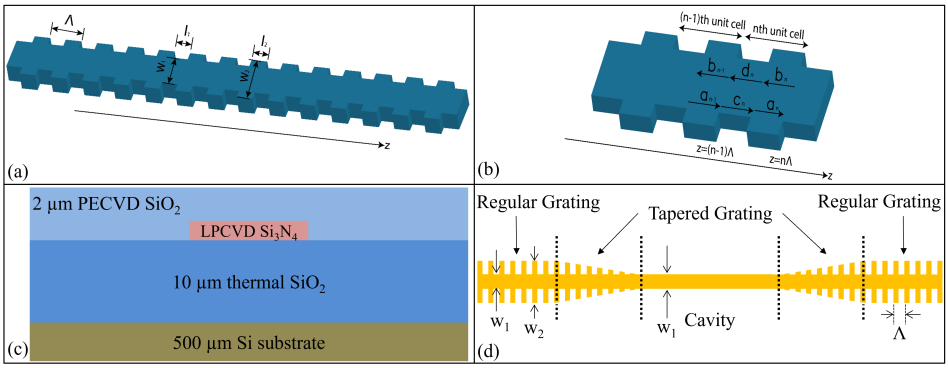

Fig. 1. (a) Schematic illustration of a typical periodic waveguide Bragg grating. (b) Complex amplitudes of the forward-travelling and backward-travelling plane waves in each layer. (c) Waveguide cross section illustration. (d) Illustration of the Fabry-Perot Bragg grating design with tapered grating.

waveguide, we can consider the light to propagate only in the z direction. A general solution to the wave equation can be formed by writing:

$$\vec{E}\,(z,t) = \vec{E}(z)e^{i\omega t} \tag{2}$$

The electric field within each layer can be expressed as a sum of a forward-traveling (+z) and a backward-travelling (-z) plane wave,

$$\vec{E}(z) = \begin{cases} a_n e^{-ik_{1z}(z-n\Lambda)} + b_n e^{+ik_{1z}(z-n\Lambda)}, & n\Lambda - l_1 < z < n\Lambda \\ c_n e^{-ik_{2z}(z-n\Lambda+l_1)} + d_n e^{+ik_{2z}(z-n\Lambda+l_1)}, & (n-1)\Lambda < z < n\Lambda - l_1 \end{cases} \tag{3}$$

with $k_{1z} = \frac{n_1\omega}{c}$, $k_{2z} = \frac{n_2\omega}{c}$, where n stands for the nth period, and a_n, b_n, c_n and d_n are constants that are related by the continuity conditions at the interfaces.

Without loss of generality, we consider a TE-like mode. By requiring the continuity of E_x and H_y at two interfaces $z = (n-1)\Lambda$ and $z = n\Lambda - l_1$, we get $\begin{bmatrix} a \\ b \end{bmatrix} = \begin{bmatrix} A & B \\ C & D \end{bmatrix} \begin{bmatrix} c \\ d \end{bmatrix}$, where

$$\begin{cases} A = \frac{1}{2k_{1z}}(k_{2z} + k_{1z})e^{ik_{2z}l_2} \\ B = -\frac{1}{2k_{1z}}(k_{2z} - k_{1z})e^{-ik_{2z}l_2} \\ C = -\frac{1}{2k_{1z}}(k_{2z} - k_{1z})e^{ik_{2z}l_2} \\ D = \frac{1}{2k_{1z}}(k_{2z} + k_{1z})e^{-ik_{2z}l_2} \end{cases} \tag{4}$$

To take the loss terms into consideration, we need to add an imaginary part to k_{1z} and k_{2z},

$$\begin{aligned} k_{1z} &= n_1 \times \frac{2\pi}{\lambda} - in_{1img} \times \frac{2\pi}{\lambda} \\ k_{2z} &= n_2 \times \frac{2\pi}{\lambda} - in_{2img} \times \frac{2\pi}{\lambda} \end{aligned} \tag{5}$$

Note that $\alpha = 4\pi n_{\mathrm{img}}/\lambda$, and we have two loss terms, the grating loss α_g and the cavity loss α_c.

Optics EXPRESS

The transfer matrix $T_i = \begin{bmatrix} A & B \\ C & D \end{bmatrix}$ is used to calculate the overall transmission T of the FBPG device, where $T = T_N T_{N-1} T_{N-2} \cdots T_2 T_1$. We further get $\begin{bmatrix} a_0 \\ b_0 \end{bmatrix} = T \begin{bmatrix} a_N \\ b_N \end{bmatrix}$. Then, the reflection and transmission coefficients of FBPG are given by $r_N = \left(\frac{b_0}{a_0}\right)_{b_N=0}$, and $t_N = \left(\frac{a_N}{a_0}\right)_{b_N=0}$.

2.2. Q vs L model

Both FPBG and micro ring resonators are types of optical resonators that rely on the constructive interference of light waves to create resonances at specific wavelengths. The main difference between FPBG and micro ring resonators is in the mechanism of resonant coupling. We take the analogy between the two resonators. Based on the model described in [15,17], we established a new model to extract the propagation loss in the FP cavity, and the coupling loss between the grating Bloch mode and the cavity mode.

We know that in the add/drop micro ring resonator, the theoretically obtainable loaded Q and intrinsic Q are,

$$Q_{load}^{ring} \approx \frac{2\pi n_{eff} L}{\lambda}[2\mathrm{K} + \alpha L + 2\gamma]^{-1} \tag{6}$$

$$Q_{int}^{ring} = \frac{2\pi n_{eff} L}{\lambda}[\alpha L + 2\gamma]^{-1} \tag{7}$$

where K is the power coupling coefficient, α is propagation loss, L is the perimeter of the ring resonator, and γ is the excess fractional power loss of the coupler.

The FPBG resonator is analogous to an add/drop ring resonator. We can equate the BG reflectance R with $1 - K$. With the cavity length of L, and the amplitude loss per scattering due to mode mismatch between the grating mode and the cavity mode, we can extract the overall amplitude round trip loss $\sigma \triangleq a^2 e^{-\alpha L}$. Since the excess power coupling loss γ is normally much smaller than unity, so that $a = \sqrt{1-\gamma} \approx 1 - (1/2)\gamma$. To simplify the calculation, we introduce the amplitude round trip factor $G \triangleq \sigma\sqrt{R_1}\sqrt{R_2}$, where R_1 and R_2 are the two reflectance of Bragg grating at both sides separately. It represents the amplitude amplification per round trip. For $R_1 = R_2 = R$,

$$G = a^2 e^{-\alpha L} R \approx (1-\gamma)(1-\alpha L)(1-(1-R)) \approx 1 - ((1-R) + \alpha L + \gamma)$$

For high Q region, where $1 - G \ll 1$, we obtain the theoretical loaded Q of FPBG as,

$$Q_{load}^{FPBG} = \frac{2\pi n_{eff} L}{\lambda}\frac{\sqrt{G}}{1-G} \approx \frac{2\pi n_{eff} L}{\lambda}\frac{1}{1-G} = \frac{2\pi n_{eff} L}{\lambda}[(1-R) + \alpha L + \gamma]^{-1} \tag{8}$$

And the intrinsic Q of FPBG is obtained when $R = 1$, as,

$$Q_{int}^{FPBG} = \frac{2\pi n_{eff} L}{\lambda}[\alpha L + \gamma]^{-1} \tag{9}$$

By measuring the Q_{load} and fitting it as a function of cavity lengths, we can extract the propagation loss α and the coupling loss γ. Furthermore, the intrinsic Q_{int} can be calculated.

3. Device design, fabrication and characterization

3.1. Device design

For the Fabry-Perot Bragg grating cavity, two different Si_3N_4 film thickness are chosen to be optimized in this work. The thickness is 100 nm and 300 nm separately, which is formed by

Optics EXPRESS

low pressure chemical vapor deposition (LPCVD), as shown in Fig. 1(c). To reduce the mode mismatch between the waveguide mode and the grating Bloch mode, an adiabatic tapered grating is added between the regular Bragg grating and the cavity (shown in Fig. 1(d)), which facilitates the adiabatic mode conversion and significantly reduces the grating-cavity coupling loss [18,19]. Instead of having a periodic variation of the width along the waveguide propagation direction, as shown in the regular grating region of Fig. 1(d), the wider width of the tapered grating, w_2, is linearly decreased to w_1 when it interconnects with the cavity. The grating period Λ stays the same inside the tapered grating and regular grating regions. By simply linearly increasing the grating width w_2, the grating loss can be reduced from 3.5 dB/cm to 0.36 dB/cm [10]. This also avoids exciting the higher order of modes in the cavity. A single grating period in this work is formed by two segments ($w_1 = 2\,\mu m$, $w_2 = 4\,\mu m$), see Fig. 1(d). The tapered grating region is implemented with 100 grating periods to achieve adiabatic mode conversion.

3.2. Device fabrication

The FPBG structure used in this paper (Fig. 1(a)) has layers of 10-μm thermal SiO_2 as the bottom cladding, 100-nm or 300-nm Si_3N_4 deposited by LPCVD as the core layer, and 2-μm SiO_2 deposited by plasma enhanced chemical vapor deposition (PECVD) as the top cladding. The FPBG design was patterned by a 100 keV Elionix ELS-G100 e-beam system. A maN-2400 negative e-beam resist film was coated as the mask to etch the Si_3N_4 layer with conductively coupled plasma (ICP) etching. Figure 2 shows the SEM images of the regular grating and the tapered grating regions of the FPBG. As we can see, a smooth sidewall is achieved with optimized ICP etching. After the deposition of the top cladding, a final thermal treatment of 12 hours at 1150 C was performed on some of the PIC chips.

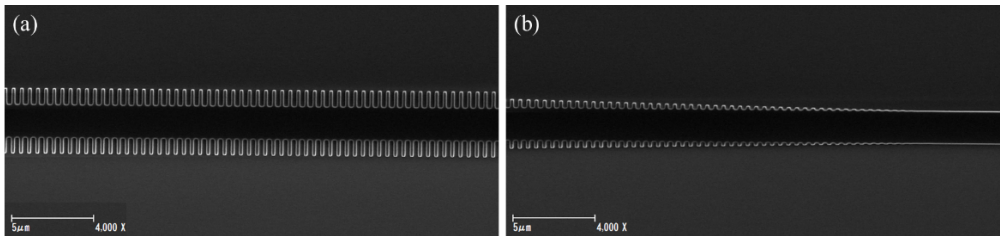

Fig. 2. SEM images of the FPBG. (a) Regular Bragg grating. (b) Linearly tapered grating connecting regular Bragg grating and cavity.

3.3. Device characterization

A polarization maintaining tunable laser source (Keysight, 81607A) operating over a wavelength range of 1450 nm − 1640 nm was used to characterize the device, see Fig. 3, which has a narrow linewidth (0.1 pm) and a high signal to total source spontaneous emission ratio (>70 dB). A polarization maintaining single mode fiber (PM1550) with a typical mode-field diameter of 10.1 μm and a numerical aperture of 0.125 was used to carry the signal from the tunable laser source to the FPBG and out to the power meter. The coupling efficiency is around ~80% with optimized butt-coupling design [20]. The polarization of the signal entering the FPBG was controlled by a high precision fiber rotator (Thorlabs, HFR007). The fibers were butt-coupled to the PIC chip using a precision 3-axis stage (< 100 nm alignment tolerance). A power meter (Keysight, N7744A) with a dynamic range of 65 dB was used to analyze the transmitted signal.

Optics EXPRESS

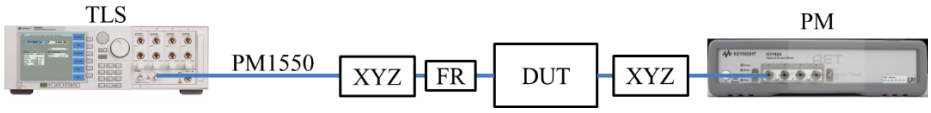

Fig. 3. A schematic of experimental set-up for the device performance measurement. TLS: tunable laser source; XYZ: motorized xyz 3-axis stage; FR: fiber rotator; DUT: device under test; PM: power meter.

4. Results and discussion

4.1. 100-nm thick Si_3N_4 platform

In Fig. 4, we show the highest quality factor measured in 100-nm thick Si_3N_4 device. The FPBG has a cavity width of 4 μm and 700 periods of Bragg grating on both sides of the cavity. In Fig. 4(a), we plot the loaded quality value Q_{load} as a function of cavity lengths. The Eq. (8) is used to fit the propagation loss α and the coupling loss γ, where R is the reflectance of the Bragg grating on each side of the cavity, L is the cavity length. The intrinsic quality factor Q_{int} can be calculated by eliminating the reflectance term, R. From the fitting results, we extract the propagation loss α to be 0.017 dB/cm, and the coupling loss γ to be 0.0005 dB. The small coupling loss is due to the tapered grating design. For the cavity length of 10 mm, the loaded quality factor Q_{load} is measured to be 10.9 million, which corresponds to an intrinsic quality factor Q_{int} 14.7 million.

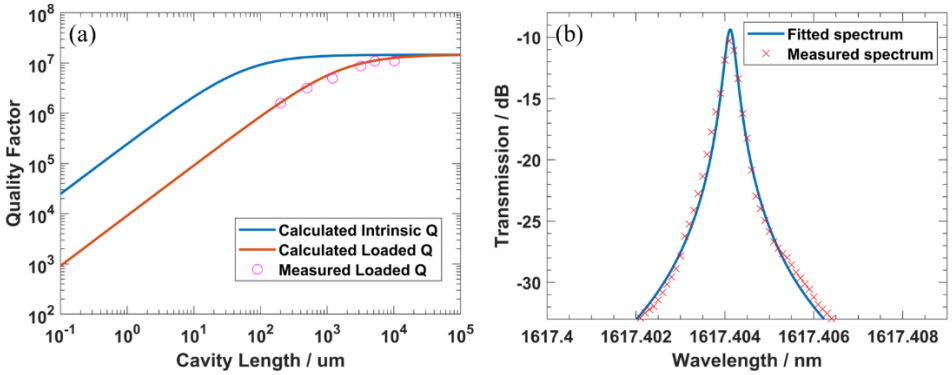

Fig. 4. 100-nm thick Si_3N_4 platform. (a) Experimental (circle) Q_{load}, calculated Q_{load} and Q_{int} as a function of Fabry-Perot cavity lengths. (b) Experimental (crossed) resonance peak fitting by transfer matrix method.

In Fig. 4(b), the transmission of the Fabry-Perot Bragg grating with 5-mm cavity length was used to fit the results by the transfer matrix method. We plot the simulation result at one of the resonance peaks with a cavity waveguide propagation loss α_c of 0.02 dB/cm, a grating propagation loss α_g of 0.25 dB/cm, and a coupling loss of 0.0005 dB. Note that α_c is the dominant factor for the Q values in the Fabry-Perot Bragg grating resonator [9].

The fitted results obtained by the two approaches, Q vs L model and ABCD transfer matrix model, are in good agreement.

To explore the effect of the waveguide core width and the annealing condition, different FPBG design and fabrication processes were performed. In Table 1, we summarized the extracted propagation losses and coupling losses under different conditions. For a FPBG device with a 2-μm wide cavity, the propagation loss is improved from 0.27 dB/cm to 0.03 dB/cm after annealed under 1150 C for 12 hours. When the width of the cavity increased to 4 μm, the propagation loss

Optics EXPRESS

is reduced to 0.11 dB/cm, compared to 0.27 dB/cm. With the thermal treatment, the propagation loss further reduced to 0.017 dB/cm. For all the devices, the grating coupling loss is extracted to be as low as 0.001 dB/pass, which is mostly due to the introduction of a tapered grating.

Table 1. 100-nm Si_3N_4 platform: FPBG loss extraction under different conditions.

Cavity width		Post-SiO_2 annealing	
		No	12 hours @1150 C
2-μm	α	0.27 dB/cm	0.03 dB/cm
	γ	0.001 dB/pass	0.001 dB/pass
4-μm	α	0.11 dB/cm	0.017 dB/cm
	γ	0.001 dB/pass	0.0005 dB/pass

4.2. 300-nm thick Si_3N_4 platform

We implemented the same grating unit ($w_1 = 2\,\mu m$, $w_2 = 4\,\mu m$) in 300-nm thick Si_3N_4 platform as in 100-nm thick Si_3N_4 platform, while the cavity width was chosen to be 2 μm, and the number of grating periods was reduced to 600 to obtain similar reflectance from the FPBG. To achieve low propagation loss, the chip was annealed under 1150 C for 10 hours. After measuring the transmitted spectrum of the fabricated devices and characterizing the loaded Q, both the Q vs L model and ABCD transfer matrix model were used to fit the experimental data, as shown in Fig. 5. The propagation loss extracted from the two models are 0.013 dB/cm and 0.014 dB/cm respectively, which are in good agreement. From the Q vs L model, we extracted the highest intrinsic quality factor Q_{int} to be 19.3 million.

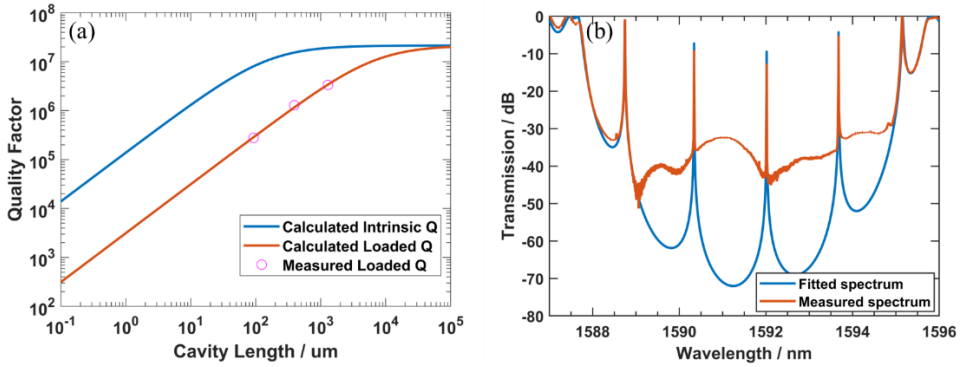

Fig. 5. 300-nm thick Si_3N_4 platform. (a) Experimental (circle) Q_{load}, calculated Q_{load} and Q_{int} as a function of Fabry-Perot cavity lengths. (b) Measured transmitted spectrum fitting by ABCD transfer matrix method.

Like the 100-nm thick Si_3N_4 platform, we observed the propagation loss reduction after the chip was annealed, from 0.07 dB/cm to 0.014 dB/cm.

4.3. Further discussion

Both the bulk material loss and the surface scattering loss contribute to the propagation loss. The thermal treatment reduces bulk loss, which includes absorption loss due to specific chemical bonds and impurities, as well as losses from internal defects, such as nano- and micro-voids. Surface scattering loss is mostly due to the mode overlapping with the interfaces, which includes top, bottom, and sidewalls. The thicker and wider cavity provides a lower propagation loss,

Optics EXPRESS

thanks to the lower overlap between the propagated mode and the interfaces of the Si_3N_4 core [2,3].

We note that lower propagation losses are also expected on thinner Si_3N_4 platform (< 60 nm) [1], as the supported mode is less confined. The delocalized mode leads to less surface scattering loss, which reduces the propagation loss significantly when the bulk material loss is minimal. However, the demonstrated high-Q resonators on thin Si_3N_4 film are mostly based on micro-ring structure. The footprint of such components is relatively large due to the limitation of critical bending radius. Since there is no bending loss concern in FPBG devices, resonators based on FPBG can be easily implemented on thin Si_3N_4 film.

5. Conclusion

An ultrahigh quality factor of 19.3 million for a Fabry-Perot Bragg grating resonator is demonstrated. Two methods, Q vs L and the transfer matrix method, have been used to extract the loss of the Si_3N_4 film. The propagation loss is as low as 0.014 dB/cm, while the coupling loss between the grating mode and the cavity mode is as low as 0.0005 dB per pass. The FPBG can be seamlessly integrated into a compact straight waveguide, requiring minimal additional space. As a result, it serves as a vital component in the construction of advanced photonic integrated circuits for various applications, enabling high-performance functionality.

Funding. National Science Foundation, National Science Foundation, Division of Electrical, Communications and Cyber Systems (2219760); Division of Astronomical Sciences (1711377); NASA Headquarters (16-APRA 16-0064, 21-APRA-21-0116).

Disclosures. The authors declare no conflicts of interest.

Data availability. Data underlying the results presented in this paper are not publicly available at this time but may be obtained from the authors upon reasonable request.

References

1. M. W. Puckett, K. Liu, N. Chauhan, Q. Zhao, N. Jin, H. Cheng, J. Wu, R. O. Behunin, P. T. Rakich, K. D. Nelson, and D. J. Blumenthal, "422 Million intrinsic quality factor planar integrated all-waveguide resonator with sub-MHz linewidth," Nat. Commun. **12**(1), 934 (2021).
2. J. Liu, G. Huang, R. N. Wang, J. He, A. S. Raja, T. Liu, N. J. Engelsen, and T. J. Kippenberg, "High-yield, wafer-scale fabrication of ultralow-loss, dispersion-engineered silicon nitride photonic circuits," Nat. Commun. **12**(1), 2236 (2021).
3. X. Ji, S. Roberts, M. Corato-Zanarella, and M. Lipson, "Methods to achieve ultra-high quality factor silicon nitride resonators," APL Photonics **6**(7), 071101 (2021).
4. W. Jin, Q.-F. Yang, L. Chang, B. Shen, H. Wang, M. A. Leal, L. Wu, M. Gao, A. Feshali, M. Paniccia, K. J. Vahala, and J. E. Bowers, "Hertz-linewidth semiconductor lasers using CMOS-ready ultra-high- Q microresonators," Nat. Photonics **15**(5), 346–353 (2021).
5. X. Ji, J. K. Jang, U. D. Dave, M. Corato-Zanarella, C. Joshi, A. L. Gaeta, and M. Lipson, "Exploiting Ultralow Loss Multimode Waveguides for Broadband Frequency Combs," Laser Photonics Rev. **15**(1), 2000353 (2021).
6. X. Ji, F. A. S. Barbosa, S. P. Roberts, A. Dutt, J. Cardenas, Y. Okawachi, A. Bryant, A. L. Gaeta, and M. Lipson, "Ultra-low-loss on-chip resonators with sub-milliwatt parametric oscillation threshold," Optica **4**(6), 619–624 (2017).
7. Y. Xuan, Y. Liu, L. T. Varghese, A. J. Metcalf, X. Xue, P.-H. Wang, K. Han, J. A. Jaramillo-Villegas, A. A. Noman, C. Wang, S. Kim, M. Teng, Y. J. Lee, B. Niu, L. Fan, J. Wang, D. E. Leaird, A. M. Weiner, and M. Qi, "High-Q silicon nitride microresonators exhibiting low-power frequency comb initiation," Optica **3**(11), 1171–1180 (2016).
8. B. Stern, X. Ji, Y. Okawachi, A. L. Gaeta, and M. Lipson, "Battery-operated integrated frequency comb generator," Nature **562**(7727), 401–405 (2018).
9. Y. Hu, Y. Zhang, P. Gatkine, J. Bland-Hawthorn, S. Veilleux, and M. Dagenais, "Characterization of Low Loss Waveguides Using Bragg Gratings," IEEE J. Sel. Top. Quantum Electron. **24**(4), 1–8 (2018).
10. S. Xie, Y. Zhang, Y. Hu, S. Veilleux, and M. Dagenais, "On-Chip Fabry–Perot Bragg Grating Cavity Enhanced Four-Wave Mixing," ACS Photonics **7**(4), 1009–1015 (2020).
11. Y. Zhao, Y. Shi, P. Dai, S. Liu, L. Hao, Y. Ma, and X. Chen, "Side-Coupled Fabry-Perot Resonator Filter Based on Dual-Waveguide Bragg Grating," J. Lightwave Technol. **40**, 1–11 (2022).
12. S. Xie, J. Zhan, Y. Hu, Y. Zhang, S. Veilleux, J. Bland-Hawthorn, and M. Dagenais, "Add–drop filter with complex waveguide Bragg grating and multimode interferometer operating on arbitrarily spaced channels," Opt. Lett. **43**(24), 6045–6048 (2018).

Optics EXPRESS

13. S. T. Winnall, A. C. Lindsay, M. W. Austin, J. Canning, and A. Mitchell, "A microwave channelizer and spectroscope based on an integrated optical Bragg-grating Fabry-Perot and integrated hybrid Fresnel lens system," IEEE Trans. Microwave Theory Tech. **54**(2), 868–872 (2006).
14. M. Xu, M. He, X. Liu, Y. Pan, S. Yu, and X. Cai, "Integrated Lithium Niobate Modulator and Frequency Comb Generator Based on Fabry-Perot Resonators," in *Conference on Lasers and Electro-Optics (2020), Paper JTh2B.27* (Optica Publishing Group, 2020), p. JTh2B.27.
15. O. Schwelb, "Transmission, Group Delay, and Dispersion in Single-Ring Optical Resonators and Add/Drop Filters - A Tutorial Overview," J. Lightwave Technol. **22**(5), 1380–1394 (2004).
16. Y. Zhang, J. Zhan, S. Veilleux, and M. Dagenais, "Silicon Nitride Fabry-Perot Bragg Grating Nanoresonator with Ultrahigh Intrinsic Q," in *Conference on Lasers and Electro-Optics (2022), Paper SM4G.7* (Optica Publishing Group, 2022), p. SM4G.7.
17. D. T. Spencer, J. F. Bauters, M. J. R. Heck, and J. E. Bowers, "Integrated waveguide coupled Si_3N_4 resonators in the ultrahigh-Q regime," Optica **1**(3), 153–157 (2014).
18. P. Lalanne, S. Mias, and J. P. Hugonin, "Two physical mechanisms for boosting the quality factor to cavity volume ratio of photonic crystal microcavities," Opt. Express **12**(3), 458–467 (2004).
19. Q. Quan, P. B. Deotare, and M. Loncar, "Photonic crystal nanobeam cavity strongly coupled to the feeding waveguide," Appl. Phys. Lett. **96**(20), 203102 (2010).
20. T. Zhu, Y. Hu, P. Gatkine, S. Veilleux, J. Bland-Hawthorn, and M. Dagenais, "Ultrabroadband High Coupling Efficiency Fiber-to-Waveguide Coupler Using Si_3N_4/SiO_2Waveguides on Silicon," IEEE Photonics J. **8**(6), 1–7 (2016).